https://doi.org/10.5194/egusphere-2023-2119
Preprint. Discussion started: 9 October 2023

An efficient approach for inverting rock exhumation from thermochronologic age-elevation relationship

Yuntao Tian[1,2*], Lili Pan[1], Guihong Zhang[1], Xinbo Yao[1]

[1] Guangdong Provincial Key Laboratory of Geodynamics and Geohazards, School of Earth Sciences and Engineering, Sun Yat-sen University, Guangzhou 510275, China

[2] Southern Marine Science and Engineering Guangdong Laboratory (Zhuhai), Zhuhai 519082, China

*Corresponding author:
Yuntao Tian
tianyuntao@mail.sysu.edu.cn

https://doi.org/10.5194/egusphere-2023-2119
Preprint. Discussion started: 9 October 2023

Abstract

This study implements the least-squares inversion method for solving the exhumation history from thermochornologic age-elevation relationship (AER) based on the linear equation among exhumation rate, thermochronologic age and total exhumation from the closure depth to the Earth surface. Modelling experiments demonstrate the significant and systematic influence of initial geothermal model, the *a priori* exhumation rate and the time interval length on the *a posterior* exhumation history. Lessons learned from the experiments include that (i) the modern geothermal gradient can be used for constraining the initial geothermal model, (ii) a relatively higher *a priori* exhumation rate would lead to systematically lower inversion results, and *vice versa*, (iii) the variance of the *a priori* exhumation rate controls the variation of the inverted exhumation history, (iv) the choice of time interval length should be optimized for resolving the potential temporal changes in exhumation. Putting together these findings, we propose a new stepwise inverse modeling strategy for optimizing the model parameters to mitigate the model dependencies on the initial parameters. Finally, we use three examples of different exhumation rates and histories for method demonstration. It is shown that our new modelling strategy produces geologically reasonable exhumation histories and geothermal gradients that are consistent with both the observed AER and modern geothermal data. The code and data used in this work is available in GitHub (https://github.com/yuntao-github/code4modelAER).

Key words: Thermochronology; Exhumation; Numerical inversion; Age-elevation relationship; Least-squares method; Geothermal model

https://doi.org/10.5194/egusphere-2023-2119
Preprint. Discussion started: 9 October 2023

1. Introduction

Rock exhumation from the Earth interior to the surface is important information for better understanding many geological problems, ranging from mountain building (e.g., Zeitler et al., 2001; Whipp Jr. et al., 2007; Cao et al., 2022) and its decay (e.g., House et al., 2001; Reiners et al., 2003b; Hu et al., 2006; Ault et al., 2019), to resource and hydrocarbon evaluation and exploration (e.g., Armstrong, 2005; McInnes et al., 2005; Yanites and Kesler, 2015), as well as the underpinning endogenic and exogenic processes and their interactions (e.g., Burbank et al., 2003; Reiners et al., 2003a; Valla et al., 2011a; Fox et al., 2015; Tian et al., 2015). Various experimental and modeling methods have been invented for estimating the rock exhumation at different crustal levels (Reiners and Brandon, 2006; e.g., Ferry and Watson, 2007; Anderson et al., 2008).

One type of the methods for estimating the rock exhumation in the middle and upper crust relies on thermochronologic cooling ages acquired from by noble gas and fission-track dating of a series of accessory minerals, such as mica Ar-Ar, apatite, zircon and titanite fission-track and (U-Th)/He analyses (e.g., Gallagher et al., 1998; Farley, 2002; Gleadow et al., 2002; Kohn et al., 2005; Reiners, 2005). Based on the closure temperature theory (Dodson, 1973), a thermochronologic cooling age records the time duration that a rock cooled through the corresponding closure temperature, which is a function of the kinematics describing fission-track annealing and noble gas diffusion, and rock cooling rate (Dodson, 1973). If the depth of the closure temperature isotherm can be estimated from the crustal temperature field, a time-averaged exhumation rate can be obtained from the cooling age.

Based on the thermochronologic method and thermo-exhumation modelling, many analytical and numerical tools have been implemented for inverting the exhumation and/or the associated cooling history. These tools have different functions, such as inverting temperature

https://doi.org/10.5194/egusphere-2023-2119
Preprint. Discussion started: 9 October 2023

history (Laslett et al., 1987; Harrison et al., 2005; Ketcham, 2005; Valla et al., 2011a; Gallagher, 2012), determining time-averaged exhumation rates (Brandon et al., 1998; Ehlers, 2005; Willett and Brandon, 2013), spatiotemporal changes in exhumation (Sutherland et al., 2009; Herman et al., 2013; Fox et al., 2014; Willett et al., 2020), and evolution of exhumation in two or three dimensions given a tectonic framework (Batt and Brandon, 2002; Braun, 2003; van der Beek et al., 2010; Valla et al., 2011b).

Convincing estimate of exhumation history for a region requires both a proper sampling strategy for thermochronologic data and a robust modeling approach for exhumation inversion, especially when the rock exhumation and its spatiotemporal changes are tectonically controlled (Ehlers and Farley, 2003; Schildgen et al., 2018). A routine and efficient sampling strategy acquires themochronologic ages from an elevation transect over a significant relief and a relatively confined spatial distance. Plotting the age versus elevation, i.e., the age-elevation relationship (AER), and analyzing the slope changes of the plot can provide first-order understanding of the exhumation history (Fitzgerald et al., 1986). Because both the underground geothermal field and closure temperature of thermochronometers are functions of the thermal advection and cooling during rock exhumation (e.g., Dodson, 1973; e.g., Brandon et al., 1998), as well as the long-wavelength topography (Stüwe et al., 1994; Braun, 2002; Ehlers and Farley, 2003), reliable estimates of exhumation rates require solving exhumation itself, together with the evolution of other influencing factors.

Fox et al. (2014) reported a linear inversion modeling method that solves exhumation history from AER, given a combination of *a priori* exhumation rates and assumed geothermal parameters. However, as shown in that study, the inverted exhumation history depends highly on these *a priori* values and geothermal assumptions. Building on that study, we here provide a

https://doi.org/10.5194/egusphere-2023-2119
Preprint. Discussion started: 9 October 2023

detailed test on the method and report an improved modeling strategy that makes use of both the AER and the modern geothermal gradient for inverting exhumation history. Other suggestions for model setup are also provided in this work.

2. Linear inversion method

Rock Exhumation from the closure depth of a thermochronometer, z_c, to the Earth's surface can be described as an integral of the exhumation ($\dot{e}$) from the cooling age (τ) to the present (Brandon et al., 1998; Fox et al., 2014). For a set of correlated bedrock samples with a shared history of exhumation rates ($\dot{\mathbf{e}}$), their thermochronologic ages ($\mathbf{A}$) and the corresponding closure depths ($\mathbf{z_c}$) can be expressed by the following equation.

$$\int_0^\tau \dot{e}\,dt = z_c \quad \Rightarrow \quad \mathbf{A}\dot{\mathbf{e}} = \mathbf{z_c}\,, \qquad \mathbf{(1)}$$

where $\mathbf{A}$ is a model matrix, with n rows (the total number of samples) and m columns (the total number of time intervals). Each row of the matrix is a discretization of a sample age, which is composed of a number of time lengths (Δt) followed by an age residual (R_i) and a number of zeros. The $\dot{\mathbf{e}}$ is a m-length vector of exhumation rates, and the $\mathbf{z_c}$ is n-length vector of closure depths.

This linear equation can be solved using the Least-Squares Regression approach assuming the Gaussian uncertainties and *a priori* mean exhumation rate ($\dot{\boldsymbol{e}}_{pr}$) and associated variance (σ_{pr}) (Tarantola, 2005; Fox et al., 2014). Such an approach requires a m*m-sized parameter covariance matrix, $\mathbf{C}$, and a n*n-sized data covariance matrix, $\mathbf{C}_\varepsilon$, which includes the uncertainties on the closure depths. These two matrices can be constructed as equations 2 and 3, respectively.

$$C_{ij} = \begin{cases} \sigma_{pr}^2, & if\ i = j \\ 0, & if\ i \neq j \end{cases} \qquad (2)$$

$$(C_\epsilon)_{ij} = \begin{cases} \dot{e}_{pr}\epsilon_i\ , & if\ i = j \\ 0, & if\ i \neq j \end{cases}, \qquad (3)$$

https://doi.org/10.5194/egusphere-2023-2119
Preprint. Discussion started: 9 October 2023

where $\dot{e}_{pr}$ and σ_{pr} are the *a priori* exhumation and the associated variance, and the ε_i is analytical uncertainty of the age data. The construction of the data covariance matrix assumes the age data are uncorrelated. Worth noting is that previous studies used different constructions of the data covariance, changing from using the analytical age uncertainties (Fox et al., 2014; Fox et al., 2015) to constant values (Jiao et al., 2017; Stalder et al., 2020).

Given the above model parameters, the equation 1 has a maximum likelihood solution for the exhumation rate vector:

$$\dot{\mathbf{e}}_{po} = \dot{\mathbf{e}}_{pr} + \mathbf{C}\mathbf{A}^T(\mathbf{A}\mathbf{C}\mathbf{A}^T + \mathbf{C}_\epsilon)^{-1}(\mathbf{z}_c - \mathbf{A}\dot{\mathbf{e}}_{pr}), \tag{4}$$

where $\dot{\mathbf{e}}_{pr}$ is a n-length vector of $\dot{e}_{pr}$, $\mathbf{z}_c$ is the n-length vector of closure depths calculated using a combination of exhumation and geothermal model parameters (see section 3). The $\dot{\mathbf{e}}_{po}$ is the posteriori maximum likelihood estimate of the exhumation rate, with a covariance matrix, $\mathbf{C}_{po}$, which provides an estimate of the uncertainties on the model parameters (equation 5).

$$\mathbf{C}_{po} = \mathbf{C} - \mathbf{C}\mathbf{A}^T(\mathbf{A}\mathbf{C}\mathbf{A}^T + \mathbf{C}_\epsilon)^{-1}\mathbf{A}\mathbf{C} \tag{5}$$

The method also provides a model resolution matrix, **R**, which gives a measure on how well the model estimates correspond to the true values:

$$\mathbf{R} = \mathbf{C}\mathbf{A}^T(\mathbf{A}\mathbf{C}\mathbf{A}^T + \mathbf{C}_\epsilon)^{-1}\mathrm{A}. \tag{6}$$

3. Closure depth and topographic correction

Inversion of the exhumation using the equation 1 requires accurate estimates of the closure depths of the thermochronologic ages ($\mathbf{z}_c$), i.e., the depth of the closure temperatures (Fig. 1). These depths can be determined from the underground temperature model, which can be simplified as and calculated by the following 1D thermal conduction and convection equation (Turcotte and Schubert, 2002):

https://doi.org/10.5194/egusphere-2023-2119
Preprint. Discussion started: 9 October 2023

$$\frac{\partial T_m}{\partial t} = \kappa \frac{\partial^2 T_m}{\partial z^2} + \dot{e}\frac{\partial T_m}{\partial z} + A_b, \tag{7}$$

where A_b is the heat production (in ºC/Myr). This function can be numerically solved using a Crank–Nicolson time integration with a set of initial and boundary conditions, such as an initial geothermal gradient (G0) at the start time of the model and surface temperature (*Ts*) (Turcotte and Schubert, 2002; Fox et al., 2014).

The closure temperature (T_c) of a thermochronometer is a function of cooling rate ($\dot{T}$) at the closure time and kinetic parameters of Helium and Argon diffusion and fission-track annealing in mineral phases (Dodson, 1973):

$$\dot{T} = \frac{\Omega R T_c^2}{E_a} \exp\left(\frac{-E_a}{R T_c}\right), \tag{8}$$

where Ω and E_a are the diffusion frequency factor normalized by the mineral size and geometry, and activation energy, respectively. Parameter R is the gas law constant. See reviews by Reiners and Brandon (2006) for the Ω and E_a parameter values for different thermochronometers.

The cooling rate ($\dot{T}$) can be computed from the derivative of transient geotherms, $T_m(t,z)$ that can be computed using equation 7 (Fox et al., 2014):

$$\dot{T} = \frac{\partial T_m}{\partial t} + \dot{e}\frac{\partial T_m}{\partial z}, \tag{9}$$

where $\dot{e}$ is unknown exhumation that can be computed through the equation 1.

Combining the equations 7-9, the closure depth of a thermochronological system ($z_{c,m}$) can be numerically computed. This depth also needs a topographic correction, because of the topographic perturbation, p, on the isotherms (Stüwe et al., 1994; Braun, 2002; Ehlers and Farley, 2003; Fox et al., 2014). Such a perturbation can be determined by the following equation:

$$p(\lambda) = \left(\frac{\gamma_0 - \gamma_a}{\gamma_{z_m}}\right) \exp\left(-z_m\left(\frac{\dot{e}}{2\kappa} + \sqrt{\left(\frac{\dot{e}}{2\kappa}\right)^2 + (2\pi\kappa)^2}\right)\right) h(\lambda), \tag{10}$$

https://doi.org/10.5194/egusphere-2023-2119
Preprint. Discussion started: 9 October 2023

where γ_a is the atmospheric lapse rate, γ_0 and γ_{z_m} are the thermal gradients at the model surface and at the depth z_m. The $h(\lambda)$ is a cosine function expression of the model surface topography, which can be determined using the discrete Fast Fourier Transform at the frequency domain. Here we use the SRTM30 data for computing the topography of regions of interests.

Finally, the closure depth of the z_c is corrected by the topographic perturbation (e.g., Brandon et al., 1998):

$$(z_c)_i = (z_{c,m})_i - p_i + h_i, \tag{11}$$

where $z_{c,m}$ is the closure depth calculated using the 1D geothermal model, p and h are the topographic perturbation and elevation difference with respect to the mean elevation at the sample site (Fig. 1), and the i denotes the i-th age.

As shown by the equations 7, 8 and 9, the closure depth is a non-linear function of rock cooling and exhumation. Therefore, the problem of interest is non-linear, which can be addressed by iterative numerical modelling methods. In this work, the solution of exhumation is approximated by coupling and iterating the linear inversion and closure depth modeling. As shown in Tarantola (2005) and Fox et al. (2014), the algorithm converges in a few iterations and produces stable outputs.

4. Model evaluation

Quantitative model assessment relies on the fitness of the predicted ages to the observed, using the following misfit function:

$$\Phi_\tau = \sqrt{\frac{1}{N}\sum_{i=1}^{N}\left(\frac{\tau_{prd,i}-\tau_{obs,i}}{\varepsilon_i}\right)^2}, \tag{12}$$

where $\tau_{obs,i}$ and $\tau_{prd,i}$ are the observed and predicted i-th age calculated from the exhumation history, and ε_i is the uncertainty of the observed i-th age. Following Fox et al. (2014), both the *a priori* and

https://doi.org/10.5194/egusphere-2023-2119
Preprint. Discussion started: 9 October 2023

a posteriori misfits, $\Phi_{\tau, pr}$ and $\Phi_{\tau, po}$, are determined for the models. The difference between these two misfit values provides a measure of the model improvements. A smaller posteriori misfit value indicates an improved data fitness, and *vice versa*.

To evaluate the geothermal parameters, we also determined the misfit value of the predicted to the observed modern geothermal gradient value using the following equation:

$$\Phi_{\gamma} = \sqrt{\left(\frac{\gamma_{prd} - \gamma_{obs}}{\varepsilon_{\gamma}}\right)^2}, \tag{13}$$

where γ_{prd} and γ_{obs} are the predicted and observed geothermal gradients, and ε_{γ} is the uncertainty of the observed value. Because the depth-temperature curves are slightly non-linear, the predicted geothermal gradient (γ_{prd}) is calculated as a mean value for the upper 1 km of the model. Similar as the assessment of age data, we also determined the *a priori* and *a posteriori* misfits, $\Phi_{\gamma, pr}$ and $\Phi_{\gamma, po}$ values for assessing the geothermal parameters.

5. The reference inverse model

Following Willett and Brandon (2013) and Fox et al. (2014), here we use the published AFT data acquired from Denali Massif (Fitzgerald et al., 1995) for method demonstration (Fig. 2a). A break-in-slope is shown by the AER at ~7-6 Ma, indicating a coeval change in slope change, i.e., the apparent exhumation rate (Fitzgerald et al., 1995), increasing from 0.17 ± 0.04 km/Myr to 1.2 ± 0.6 km/Myr (Fig. 2b). AER regression of young dates from the lower part of the transect (between 4.3-2.0 km) also predicts a closure depth that is the intercept at -3.3 ± 3.4 km (Fig. 2b). However, using the present geothermal gradient (38.9 °C/km) (Fox et al., 2014) and a nominal closure temperature of AFT method (110 °C) (Reiners and Brandon, 2006) and a -12 °C surface

https://doi.org/10.5194/egusphere-2023-2119
Preprint. Discussion started: 9 October 2023

temperature (Fox et al., 2014), the closure depth is predicted as ~3.1 km beneath the mean elevation (~4 km), which is equivalent to an elevation of ~0.9 km. This closure depth is significantly higher than the intercept (-3.3 ± 3.4 km). Such a difference indicates the AER slope of the lower part overestimates the exhumation rates since ~7-6 Ma.

Same as used in Fox et al. (2014), the reference inverse model uses the following parameters, a start time at 25 Ma, a time interval (Δt) of 2.5 Myr, a 4020 m mean elevation, a -12 °C surface temperature, *a priori* exhumation rate of 0.5 ± 0.15 km/Myr, a 24 °C/km initial geothermal gradient, a 38.9 °C/km present geothermal gradient, a model block with a thickness of 80 km, and a 30 km^2/Myr thermal diffusivity.

The exhumation history output of the reference model is shown in Fig. 3. The inversion results reveal an abrupt triple-four-fold increase of exhumation rate to a value of 0.55-0.7 km/Myr at 7.5 Ma (Fig. 3b), consistent with the development of the break-in-slope in the AER. The model also shows a gradual decrease of exhumation rate from *a priori* exhumation rate (0.5 km/Myr) to 0.15 km/Myr from 25 Ma to 10 Ma. The invariant exhumation during the starting stage resulted from the fact that all ages are younger than 17.5 Ma, and thus the data have no resolution for the time span. These results are similar to those of Fox et al. (2014). The posteriori misfit for the age is 1.73, significantly smaller than that of the priori model (4.68), suggesting the improvement by the inverse modeling (Fig. 3b). Such a model also provides reasonable fit to the modern temperature field, as shown by the small misfit (0.01) in the geothermal gradient (Fig. 3b).

The resolution of the inverted exhumation history can be assessed by the resolution matrix **R** (equation 6). Imaging of the matrix shows the model provides no resolution for the time period before 17.5 Ma (Fig. 3c), consistent with the fact that the youngest input age is younger than 16.1 ± 0.9 Ma. For the time span between 15 and 5 Ma, the model resolution is high, as shown by the

https://doi.org/10.5194/egusphere-2023-2119
Preprint. Discussion started: 9 October 2023

diagonal elements of the matrix, with the highest resolution at 7.5-5 Ma span, including eight age date points (Fig. 3c). The most recent two phases of exhumation (5-0Ma) are less resolved, as no ages fall into this time interval, as shown by the nearly equal resolution values for the two phases, i.e., the latest four pixels of the matrix (Fig. 3c). The modeled exhumation results for the time interval are thus time-averaged values. The slight decrease in the last stage reflects changes in geothermal gradient.

For assessing the correlation among model parameters, the calculated covariance matrix is scaled by the diagonal covariance matrix:

$$\hat{C}_{\xi\beta} = \frac{C_{\xi\beta}}{\sqrt{C_{\xi\xi}}\sqrt{C_{\beta\beta}}}\,. \tag{14}$$

The correlation matrix for the reference model is shown in Fig. 3d. The diagonal correlation values are 1 and off-diagonal ones are dominantly negative, indicating anti-correlated uncertainties (Fig. 3d), which suggests exhumation parameters were not resolved independently by the modeling. In fact, it is expected to have the anti-correlation, because, given two steps of rock exhumation, decreasing the exhumation during one step would increase that of the other step.

6. Dependence on model parameters and proposed solutions

Here we use the Denali data set for demonstrating the influences of (1) the initial geothermal parameters, (2 and 3) the *a priori* mean and variance values of the exhumation rates, and (4) time interval length on the inverted exhumation history. Also discussed in this section are the solutions for optimizing the model setup for these parameters.

6.1. Dependence on initial thermal model

https://doi.org/10.5194/egusphere-2023-2119
Preprint. Discussion started: 9 October 2023

Different initial model geothermal parameters would lead isotherms to shift either downward to greater depths or upwards to the Earth surface, and either compression or expansion among isotherms. Therefore, the initial thermal models have systematic influence on the closure depths and consequently the *a posterior* exhumation.

This is demonstrated by modelling experiments presented in Figure 4. Using a relatively lower initial geothermal gradient produces relatively higher *a posterior* exhumation rates (comparing the models shown in Figs. 4a-4f), and *vice versa*. Such an influence is significant even for the time and elevation intervals with multiple age constraints (10-5.0 Ma). For example, using relatively lower geothermal gradients of <22 ^{o}C/km would yield significantly higher average exhumation rates of >0.8 km/Myr for the last two stages (<5 Ma) (Figs. 4a-4c) than those (<0.6 km/Myr) using higher initial geothermal gradients of ≥26 ^{o}C/km (Figs. 4d-f). Worth noting is that the models using relatively lower (16-20 ^{o}C/km, Figs. 4a-4b) and higher (30-34 ^{o}C/km, Figs. 4e-4f) initial geothermal gradients yield relatively worse misfits (>1) than those using medium initial gradients (22-26 ^{o}C/km) (Figs. 3 and 4c-4d), suggesting that the modern geothermal gradient can be used as a constraint for the initial geothermal model.

These results highlight the importance of taking geothermal parameters into account in inverting the exhumation history. We proposed to run a set of models using different *a priori* geothermal parameters, especially the initial geothermal gradient, to search for the proper intitial geothermal setup that provides reasonable fits to both the ages and the modern geothermal gradient (see section 7 for details).

6.2. Dependence on the *a priori* exhumation rate

https://doi.org/10.5194/egusphere-2023-2119
Preprint. Discussion started: 9 October 2023

Both the mean and variance of the *a priori* exhumation rate have important influences on the model solution for the maximum likelihood estimation method. Our modeling experiments show that the mean value of the *a priori* exhumation has systematic influences on the inverted exhumation. Similar to the reference model, exhumation of the preceding three stages (25-17.5 Ma) without age constraints is the same as the *a priori* input. For the following stages, a relatively higher mean value of the *a priori* exhumation results in relatively lower *a posterior*i exhumation rates (comparing different models presented in Fig. 5). For example, models using the mean *a priori* exhumation of ≤0.4 km/Myr yield *a posterior* exhumation of 0.55-0.8 km/Myr for the stages <7.5 Ma (Figs. 5a-5c), whereas those using a higher *a priori* value (≥ 0.6 km/Myr) result in *a posterior* exhumation of 0.45-0.7 km/Myr for the same stages (Figs. 5d-5f). This is because a relatively higher *a priori* value, which would be used for calculating thermal models, would lead to a quicker increase in geothermal gradient and thus relatively shallower closure depths and relatively lower exhumation rates.

The variance of the *a priori* exhumation rate has important influence on both the exhumation rates and the posterior variance. Models with lower *a priori* variances yield less variations in the *a posterior* exhumation history, and *vice versa* (comparing models in Fig. 6). Further, models using the input variance of the *a priori* exhumation of 0.2-0.3 km/Myr (40-60% of the mean value), the variation of the inverted exhumation history becomes stable (Figs. 3, 6c-6d). Given that the uncertainty of the input age data, which is often 10%-20% at a two-sigma level, larger variance of the inverted exhumation would be unreasonable (Figs. 6e-6f), especially when multiple age data are available at different elevations.

We proposed to run a set of models using different *a priori* mean value of erosion rates to search for the one that provides appropriate fits to both the ages and the modern geothermal

https://doi.org/10.5194/egusphere-2023-2119
Preprint. Discussion started: 9 October 2023

gradient. As to the *a priori* variance of erosion rates, we propose to use a relative uncertainty of 30-70% of the mean value. Larger *a priori* variance would lead to larger uncertainties for the exhumation rates, which is unreasonable and non-meaning for geological studies.

6.3. Dependence on time interval length

Constraining the onset time of major changes in exhumation rates is one of the important tasks for inverting the exhumation history from thermochronologic data. Using a large time length cannot accurately capture the potential transition time of exhumation rates. As shown in the Figs. 7b-7d, models using time lengths of ≤3.5 Ma show an abrupt increase in exhumation at 7-6 Ma, consistent with that shown in AER plot. However, the models using a large time length (≥4.5 Ma) overestimate the onset time of the enhanced exhumation (Figs. 7e-7f). Further, a relatively shorter time length would smooth temporal changes in exhumation rates, leading to an underestimating of the variations. For example, as shown in the Fig. 7a, the model using a relatively shorter time length (0.5 Ma) yields an exhumation variation between 0.35-0.60 km/Myr, significantly lower than those using relatively larger time interval lengths (Figs. 7b-7f). In addition, a shorter time length also significantly increases the computational time and resources, especially when processing a large number of vertical transects.

Given the interests in major exhumation changes, we propose the time interval length (Δt) should be optimized for constraining the transitional time and the associated exhumation changes. Therefore, the time interval length should be set as the absolute uncertainty at two sigma levels at the break point (τ_b) (equation 15). If the break point is unclear in AER, we propose to use the absolute uncertainty at two-three sigma levels at the median age value ($\tilde{\tau}$) (equation 15), so as to focus on the time intervals where ages cluster.

https://doi.org/10.5194/egusphere-2023-2119
Preprint. Discussion started: 9 October 2023

$$\Delta\tau = \begin{cases} \delta\tau_b, & if\ a\ break\ in\ slope\ exists \\ \delta\tilde{\tau}, & if\ no\ clear\ break\ in\ AER \end{cases}, \tag{15}$$

where δ is the relative age uncertainty at two sigma levels, varying between 10%-20% among different studies. Following this method, the Denali case should use a time length of ~1.5 Ma (7 Ma × 20%), slightly lower than that used in the reference model (Fig. 3).

7. A new modeling strategy

Putting together the lessons learned from the above modelling experiments, a new stepwise modeling strategy develops for addressing the model dependencies on the initial geothermal parameter, the *a priori* exhumation rates and time interval length. As illustrated in the Figure 8, the approach includes the following three steps.

(i) Estimating a time-averaged erosion rate. Dividing each nominal closure depth, which can be estimated from the nominal closure temperatures and the modern geothermal gradient, by the corresponding age results in a time-averaged erosion rate. Then, a mean value can be determined by averaging the rates. Such a mean value and assumed variance (50% in this work) will be used as the *a priori* erosion rate.

(ii) Optimizing the fit to the modern geothermal gradient. This step runs a set of inversion models (20 in this work) using different geothermal gradients, ranging from 60% to 120% of the modern value, together with the *a priori* erosion rate estimated in the first step, for determining the initial geothermal gradient that yields the maximum fit to the modern value, i.e., the minimum Φ_γ (equation 13).

(iii) Optimizing the fit to both the age data and the geothermal gradient. Given the model dependence on the geothermal parameters (see section 6.1), a comprehensive evaluation of the models should assess not only the age misfit (Φ_τ), but also that of the geothermal gradient (Φ_γ). In

https://doi.org/10.5194/egusphere-2023-2119
Preprint. Discussion started: 9 October 2023

the third step, a set of inversion models (20 in this work) are run using different *a priori* erosion rates, changing from 20% to 150% of the mean value estimated in the first step, together with the estimated geothermal gradient by the second step, to search for the model that provides the best fit to both the age data and the modern geothermal gradient. This study uses the following compound misfit function to evaluate the models:

$$\Phi = \Phi_\tau + \Phi_\gamma/\sqrt{N}, \quad (17)$$

where Φ_τ and Φ_γ are misfit values for the age and geothermal gradient calculated using the equations 12 and 13, and N is the number of age inputs. Dividing Φ_γ by the square root of N in this equation, as also done for calculating the Φ_τ (equation 12), means that the modern geothermal gradient is given the same weight as an age input for evaluating the model.

8. Examples for testing the new modeling strategy

Below we use three examples to demonstrate our new method. The Denali data is used again for demonstrating the efficiency of our method. Then, we further test our method using the Himalayan Dhanladar range and KTB borehole (the Continental Deep Drilling Project in Germany) thermochronologic data for representing regions of fast and slow erosion, respectively.

8.1 The Denali transect

Using the stepwise inversion modeling strategy, the Denali transect yields an exhumation history generally similar with that of the reference model. Differences in the *a priori* parameters include that the new inversion finds and uses an initial geothermal gradient of 24.57 ^{o}C/km (slightly higher than that of the reference model), *a priori* erosion rate of 0.36 ± 0.18 km/Myr (slightly lower than that of the reference model) and a time interval length of 1.5 Ma. The combination of these *a priori* parameters result in erosion rates of 0.65-0.70 km/Myr since 6 Ma,

https://doi.org/10.5194/egusphere-2023-2119
Preprint. Discussion started: 9 October 2023

which is slightly latter than that of the reference model. The subtle differences from the reference model mainly result from the time interval length used in different models. Comparing the misfit values, the new model produces slightly better fits than the reference model, with the *a posterior* misfit values of 1.66 and 0.0) for the observed age and geothermal data (Fig. 9a).

8.2 Himalayan Dharladar range transect

AFT and ZHe data from the Dharladar range in the central Himalayas, reported in the publications by Deeken et al. (2011) and Thiede et al. (2017) are used as an example for regions of young cooling ages and fast exhumation. The samples were collected in an elevation range between 1.5 and 4.5 km, covering a topographic relief of 3 km within a spatial distance of ~15 km on the hanging wall of the main central thrust of the Himalayan fold-thrust-belt (Deeken et al., 2011; Thiede et al., 2017). AER slope regression suggests an increase in apparent erosion rates from ~0.2 km/Myr to ~2.8 km/Myr at ~3.7-6.4 Ma (Deeken et al., 2011). Using geothermal gradients of 25-45 ^{o}C/km, time-averaged erosion rates were estimated as 0.8-2.0 km/Myr and 0.8-1.7 km/My since 3.7 Ma and 14.5 Ma, respectively (Deeken et al., 2011).

The modelling of the Dharladar range data uses a modern geothermal gradient constraint of 45 ± 8 ^{o}C/km (Deeken et al., 2011). The relatively large uncertainty is assigned for the geothermal gradient, because of the absence of direct geothermal measurements in the study area. Our exhumation inversion for the AER data using the stepwise modeling strategy yields relatively slow rates of 0.2-0.4 km/Myr and relatively fast rates of 1.3-1.5 km/Myr before and after 6-5 Ma, respectively (Fig. 9b). The abrupt increase of exhumation rates at 6-5 Ma is generally consistent with the estimates from the slope regression results of Deeken et al. (2011). The modelling yields a history of the geothermal gradient that gradually increases to a modern value of ~44 °C/km, close to the input value (45 ± 8 °C/km).

8.3 KTB borehole

The KTB borehole yields a large thermochornologic and geochronologic age data (Warnock and Zeitler, 1998; Stockli and Farley, 2004; Wolfe and Stockli, 2010). Previous studies suggest the borehole are truncated by multiple faults, which offset the age-depth relationship (Wagner et al., 1997). Here we use the data at depths shallower than 1 km, where data are abundant and have linear relationship with depths.

The KTB apatite, zircon and titanite (U-Th)/He (AHe, ZHe and THe) and AFT age data vary largely between 85-50 Ma. These clustered ages have been interpreted as indicating a late Cretaceous phase of exhumation, followed by slow exhumation (Wagner et al., 1997; Stockli and Farley, 2004), as also shown by previous thermal history reconstructions based on k-feldspar $^{40}Ar/^{39}Ar$ data (Warnock and Zeitler, 1998).

Our modeling, using the AER data and a modern geothermal gradient of 27.5 ± 2.8 °C/km (Clauser et al., 1997), shows that elevated exhumation rates (0.12-0.15 km/Myr) between 80-60 Ma, followed by slower exhumation rates of ~0.04 km/Myr (Fig. 9c), are similar to previous estimates (Wagner et al., 1997; Warnock and Zeitler, 1998; Stockli and Farley, 2004). Associated with changes in exhumation, geothermal gradient gradually decreases from the peak values at 70-60 Ma to a value of ~28 °C/km at the present-day.

9. Conclusion

https://doi.org/10.5194/egusphere-2023-2119
Preprint. Discussion started: 9 October 2023

The *a priori* information has important effects on the inversion results using the least-squares inversion method. Our study demonstrates the importance of geothermal gradient and the *a priori* exhumation rate in estimating the exhumation history from the thermochronology data. To take into account the geothermal data into the exhumation history inversion, we propose a stepwise inversion model strategy that first searches for the appropriate initial geothermal gradient, which will then be used in the modelling searching for the *a priori* exhumation rate. Our modelling strategy produces exhumation history and geothermal gradient that provide reasonable fits for both the observed AER and modern geothermal data. The code and data used in this work are available in GITHUB.

Code availability

The code used in this work are available in GITHUB (https://github.com/yuntao-github/code4modelAER).

Data availability

The data used in this work are available in GITHUB (https://github.com/yuntao-github/code4modelAER).

Author contribution

Yuntao Tian: Conceptualization, Methodology, Software, Data curation, Visualization, Investigation, Writing- Original draft preparation. Lili Pan: Visualization, Writing- Reviewing and Editing. Guihong Zhang and Xinbo Yao: Writing- Reviewing and Editing.

https://doi.org/10.5194/egusphere-2023-2119
Preprint. Discussion started: 9 October 2023

Competing interests

The contact author has declared that none of the authors has any competing interests.

Acknowledgments

This study is funded by the National Natural Science Foundation of China (42172229, 41888101 and 41772211). Discussions with Jie Hu and Donglan Zeng are gratefully appreciated.

References:

Anderson, J.L., Barth, A.P., Wooden, J.L. et al., 2008. Reviews in Mineralogy and Geochemistry, 69(1): 121-142.
Armstrong, P.A., 2005. Reviews in mineralogy and geochemistry, 58(1): 499-525.
Ault, A.K., Gautheron, C. and King, G.E., 2019. Tectonics, 38(11): 3705-3739.
Batt, G.E. and Brandon, M.T., 2002. Tectonophysics, 349(1-4): 185-201.
Brandon, M.T., Roden-Tice, M.K. and Garver, J.I., 1998. Bulletin of the Geological Society of America, 110(8): 985-1009.
Braun, J., 2002. Earth and Planetary Science Letters, 200(3-4): 331-343.
Braun, J., 2003. Computers & Geosciences, 29(6): 787-794.
Burbank, D.W., Blythe, A.E., Putkonen, J. et al., 2003. Nature, 426(6967): 652-655.
Cao, K., Tian, Y., van der Beek, P. et al., 2022. Earth-Science Reviews: 104160.
Clauser, C., Giese, P., Huenges, E. et al., 1997. Journal of Geophysical Research: Solid Earth, 102(B8): 18417-18441.
Deeken, A., Thiede, R.C., Sobel, E.R. et al., 2011. Earth and Planetary Science Letters, 305(1-2): 103-114.
Dodson, M.H., 1973. Contributions to Mineralogy and Petrology, 40(3): 259-274.
Ehlers, T.A., 2005. Reviews in Mineralogy and Geochemistry, 58(1): 315-350.
Ehlers, T.A. and Farley, K.A., 2003. Earth and Planetary Science Letters, 206(1-2): 1-14.
Farley, K.A., 2002. Reviews in Mineralogy and Geochemistry, 47(1): 819-844.
Ferry, J.M. and Watson, E.B., 2007. Contributions to Mineralogy and Petrology, 154(4): 429-437.
Fitzgerald, P.G., Sandiford, M., Barrett, P.J. et al., 1986. Earth and Planetary Science Letters, 81(1): 67-78.
Fitzgerald, P.G., Sorkhabi, R.B., Redfield, T.F. et al., 1995. Journal of Geophysical Research: Solid Earth, 100(B10): 20175-20191.
Fox, M., Herman, F., Kissling, E. et al., 2015. Geology, 43(5): 379-382.
Fox, M., Herman, F., Willett, S.D. et al., 2014. Earth Surf. Dynam., 2(1): 47-65.
Gallagher, K., 2012. J. Geophys. Res., 117, B02408, doi:10.1029/2011JB008825.

https://doi.org/10.5194/egusphere-2023-2119
Preprint. Discussion started: 9 October 2023

Gallagher, K., Brown, R. and Johnson, C., 1998. Annual Review of Earth and Planetary Sciences, 26(1): 519-572.

Gleadow, A.J.W., Belton, D.X., Kohn, B.P. et al., 2002. Reviews in Mineralogy and Geochemistry, 48: 579-630.

Harrison, T.M., Grove, M., Lovera, O.M. et al., 2005. Reviews in mineralogy and geochemistry, 58(1): 389-409.

Herman, F., Seward, D., Valla, P.G. et al., 2013. Nature, 504(7480): 423-426.

House, M.A., Wernicke, B.P. and Farley, K.A., 2001. American Journal of Science, 301(2): 77-102.

Hu, S.B., Raza, A., Min, K. et al., 2006. Tectonics,25, T C6009, doi:10.1029/2006TC001985.

Jiao, R., Herman, F. and Seward, D., 2017. Earth-Science Reviews, 166: 286-298.

Ketcham, R.A., 2005. Reviews in mineralogy and geochemistry, 58(1): 275-314.

Kohn, B.P., Gleadow, A.J.W., Brown, R.W. et al., 2005. Reviews in mineralogy and geochemistry, 58(1): 527-565.

Laslett, G., Green, P.F., Duddy, I. et al., 1987. Chemical Geology, 65(1): 1-13.

McInnes, B.I.A., Evans, N.J., Fu, F.Q. et al., 2005. Reviews in mineralogy and geochemistry, 58(1): 467-498.

Reiners, P.W., 2005. Reviews in mineralogy and geochemistry, 58(1): 151-179.

Reiners, P.W. and Brandon, M.T., 2006. Annual Review of Earth and Planetary Sciences, 34: 419-466.

Reiners, P.W., Ehlers, T.A., Mitchell, S.G. et al., 2003a. Nature, 426(6967): 645-7.

Reiners, P.W., Zhou, Z.Y., Ehlers, T.A. et al., 2003b. American Journal of Science, 303(6): 489-518.

Schildgen, T.F., van der Beek, P.A., Sinclair, H.D. et al., 2018. Nature, 559(7712): 89-93.

Stalder, N.F., Herman, F., Fellin, M.G. et al., 2020. Earth-Science Reviews, 210: 103276.

Stockli, D.F. and Farley, K.A., 2004. Chemical Geology, 207(3): 223-236.

Stüwe, K., White, L. and Brown, R., 1994. Earth and Planetary Science Letters, 124(1–4): 63-74.

Sutherland, R., Gurnis, M., Kamp, P.J.J. et al., 2009. Geosphere, 5(5): 409-425.

Tarantola, A., 2005.

Thiede, R., Robert, X., Stübner, K. et al., 2017. Lithosphere, 9(5): 715-725.

Tian, Y., Kohn, B.P., Hu, S. et al., 2015. Geophysical Research Letters, 42(1): 29-35.

Turcotte, D. and Schubert, G., 2002.

Valla, P.G., Shuster, D.L. and van der Beek, P.A., 2011a. Nature Geosci, 4(10): 688-692.

Valla, P.G., van der Beek, P.A. and Braun, J., 2011b. Earth and Planetary Science Letters, 307(3-4): 309-322.

van der Beek, P.A., Valla, P.G., Herman, F. et al., 2010. Earth and Planetary Science Letters, 296(1-2): 9-22.

Vermeesch, P., 2018. Geoscience Frontiers, 9(5): 1479-1493.

Wagner, G.A., Coyle, D.A., Duyster, J. et al., 1997. Journal of Geophysical Research: Solid Earth, 102(B8): 18221-18232.

Warnock, A.C. and Zeitler, P.K., 1998. Earth and Planetary Science Letters, 158(1): 67-79.

Whipp Jr., D.M., Ehlers, T.A., Blythe, A.E. et al., 2007. Tectonics, 26, TC3003, doi:10.1029/2006TC001991.

Willett, S.D. and Brandon, M.T., 2013. Geochemistry, Geophysics, Geosystems, 14(1): 209-222.

Willett, S.D., Herman, F., Fox, M. et al., 2020. Earth Surf. Dynam. Discuss., 2020: 1-78.

Wolfe, M.R. and Stockli, D.F., 2010. Earth and Planetary Science Letters, 295(1-2): 69-82.
Yanites, B.J. and Kesler, S.E., 2015. Nature Geoscience, 8(6): 462-465.
Zeitler, P., Meltzer, A., Koons, P. et al., 2001. GSA Today, 11: 4-9.

https://doi.org/10.5194/egusphere-2023-2119
Preprint. Discussion started: 9 October 2023

Figures captions:

Figure 1. Schematics showing the relationship among closure depth (z_c), topography and its perturbation (p). The parameter h denotes the difference between the sample and the mean elevation, and z_m the depth of the closure temperature (T_c, the lower dashed line) derived from the mean elevation (upper dashed line) and intial temperature field ($T_{initial}$) and exhumation history ($\dot{e}$).

Figure 2. (a) Distribution of AFT age data (pentagons, colored by age values) over the elevation contour map computed using the SRTM30 data of the Denali massif in Alaska. AFT data sourced from Fitzgerald et al. (1995). (b) AER and the slope fitting results using isoplotR (Vermeesch, 2018). AER fitting of ages older than 6.7 Ma yields a slope of 0.17 ± 0.04 km/Myr; whereas the fitting of ages between 6.5 Ma and 4.3 Ma produces a slope of 1.2 ± 0.6 km/Myr and an intercept at -3.3 ± 3.4 km. The upper and lower dashed lines denote the mean elevation (4.02 km) and the depth of the nominal closure temperature (110 °C), calculated using the modern geothermal gradient (38.9 °C/km) and the surface temperature (-12 °C).

Figure 3. Inputs and outputs of the reference model for the Denali AFT. (a) Comparison between the observed (in black) and predicted (in blue) AER. (b) The *a posterior* exhumation history generated by the reference model. Thick and thin lines are the mean and one standard deviation of the inverted exhumation history. The red dash and solid lines are the history of the geothermal gradients, predicted by the *a priori* and *a posterior* models, respectively. (c) and (d) Plots of the resolution and correlation matrix.

https://doi.org/10.5194/egusphere-2023-2119
Preprint. Discussion started: 9 October 2023

Figure 4. Histories of exhumation and geothermal gradients, predicted by models using different *a priori* geothermal gradients between 18 ºC/km and 34 ºC/km. The blue thick and thin lines are the mean and one standard deviation of the inverted exhumation history. The red dash and solid lines are the history of the geothermal gradients, predicted by the *a priori* and *a posterior* models, respectively. Except for the initial geothermal gradient, other parameters are the same as the reference model. Comparing to the reference model which used an initial geothermal gradient of 24 ºC/km (Fig. 3), models using a lower initial geothermal gradient yield relatively higher exhumation rates (panels a-c), whereas those using a higher gradient produce lower exhumation rates (panels d-f).

Figure 5. Histories of exhumation and geothermal gradients, predicted by models using different *a priori* mean values of the exhumation rates, ranging from 0.1 km/Myr to 0.9 km/Myr. Other parameters are the same as the reference model. For explanation of the plotted lines, see Figure 4. Comparing to the reference model which used *a priori* mean exhumation of 0.5 km/Myr (Fig. 3), models using a lower *a priori* exhumation yield relatively higher exhumation rates for the last three stages (7.5 - 0 Ma) (panels a-c), whereas those using a higher *a priori* exhumation produce lower exhumation rates for the last three stages (panels d-f).

Figure 6. Histories of exhumation and geothermal gradients, predicted by models using different *a priori* variance values (between 0.05 km/Myr and 0.5 km/Myr) of the exhumation rates (0.5 km/ Myr). Other parameters are the same as the reference model. For explanation of the plotted lines, see Figure 4. Comparing to the reference model which used *a priori* variance of the exhumation (0.25 km/Myr) (Fig. 3), models using a lower *a priori* variance yield limited

https://doi.org/10.5194/egusphere-2023-2119
Preprint. Discussion started: 9 October 2023

variations and uncertainties in exhumation (panels a-c), whereas those using a higher *a priori* variance produce larger variations and uncertainties (panels d-f).

Figure 7. Histories of exhumation and geothermal gradients, predicted by models using different time interval lengths. Other parameters are the same as the reference model. For explanation of the plotted lines, see Figure 4. Comparing to the reference model which used a time interval length of 2.5 Ma (Fig. 3), models using smaller time interval lengths yield lower variations in exhumation (panels a-c) than other using larger time interval lengths (panels d-f).

Figure 8. Flow chat of the proposed stepwise modeling strategy, which includes three main steps. The first step estimates a mean exhumation rate (e0) using the nominal closure temperatures, modern geothermal gradient and sample ages. The mean rate is used in the second step which runs a set of models using different initial geothermal gradients for optimizing the initial geothermal model. The third step runs a set of models using different *a priori* exhumation rates, which is generated around the mean rate, and the optimized initial geothermal model by the second step, to find the best model that yields the minimum misfit to both age data and modern geothermal gradient.

Figure 9. The best-fit model for the Denali (a), Dhanladar range (b) and upper KTB (c) transects, using the modeling strategy shown in figure 8. First row: Comparison between the observed (in black) and predicted (in blue) AER. Second row: plots of observed and modeled ages. Third row: Histories of exhumation and geothermal gradients. The blue thick and thin lines are the mean and one standard deviation of the inverted exhumation history. The red dash and solid lines are the

https://doi.org/10.5194/egusphere-2023-2119
Preprint. Discussion started: 9 October 2023

history of the geothermal gradients, predicted by the *a priori* and *a posterior* models, respectively. Fourth and bottom row: Plots of the resolution and correlation matrix.

https://doi.org/10.5194/egusphere-2023-2119
Preprint. Discussion started: 9 October 2023

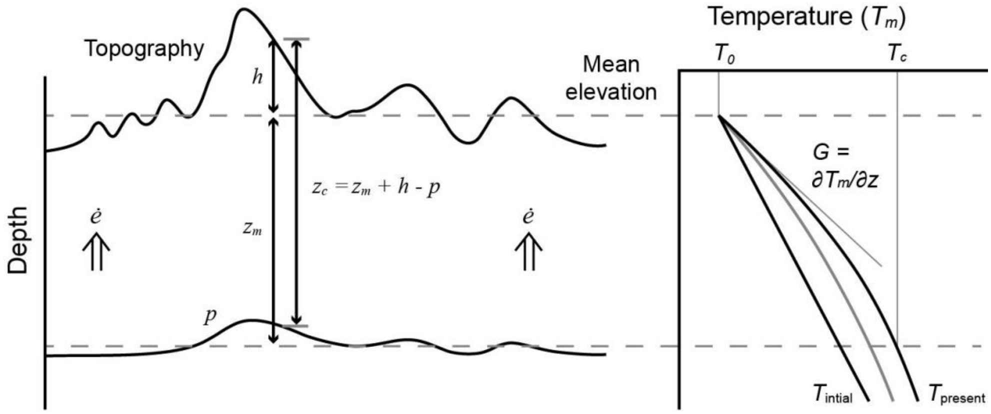

Figure 1

https://doi.org/10.5194/egusphere-2023-2119
Preprint. Discussion started: 9 October 2023

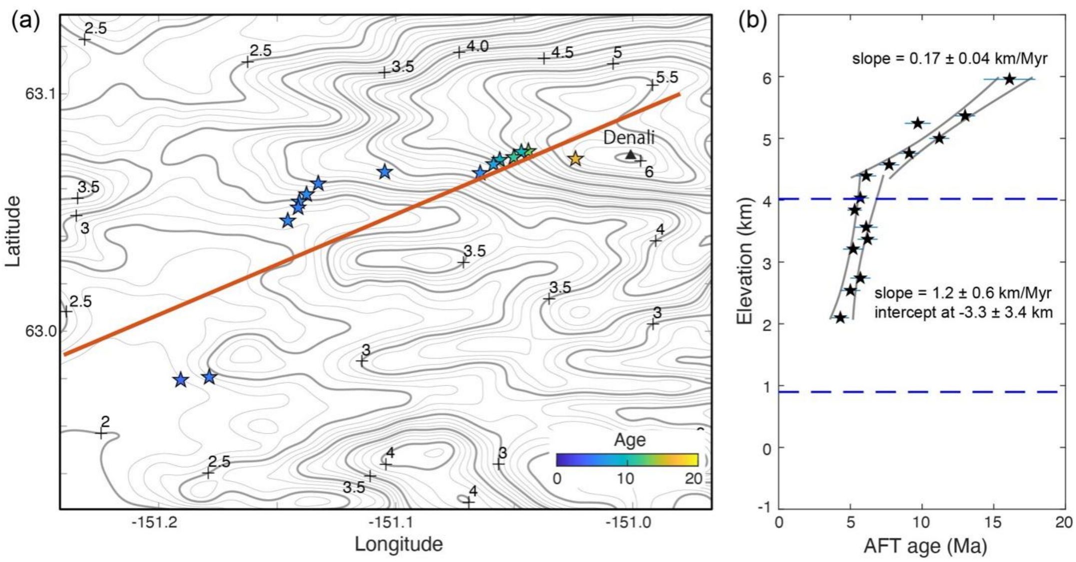

7

8 Figure 2

9

https://doi.org/10.5194/egusphere-2023-2119
Preprint. Discussion started: 9 October 2023

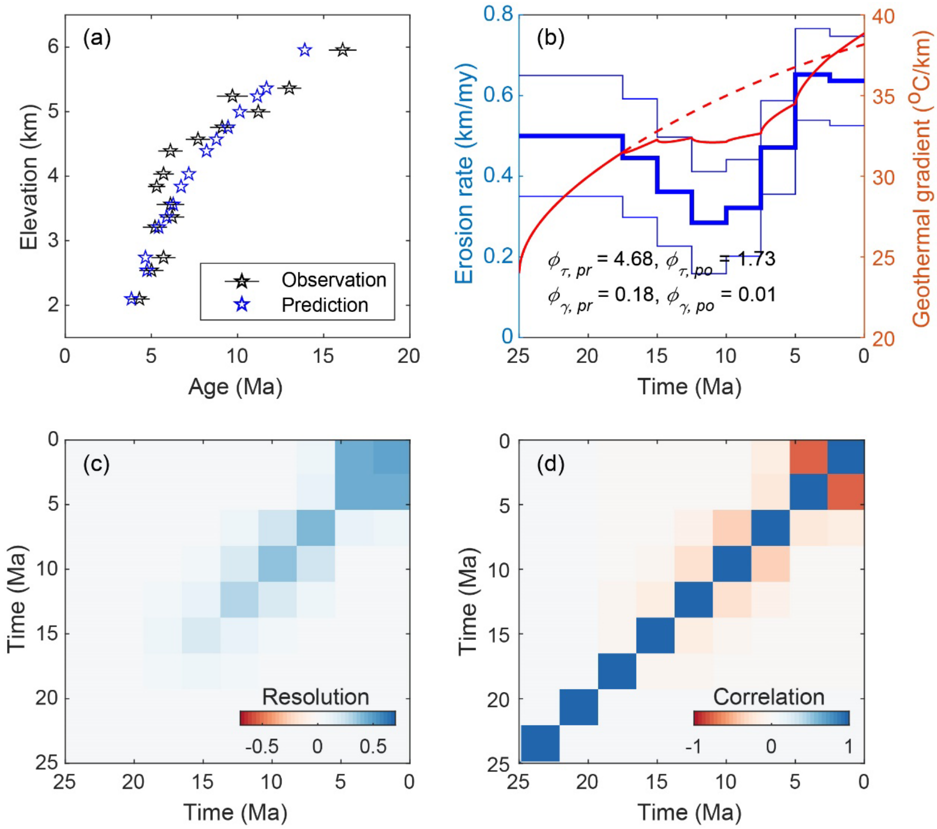

Figure 3

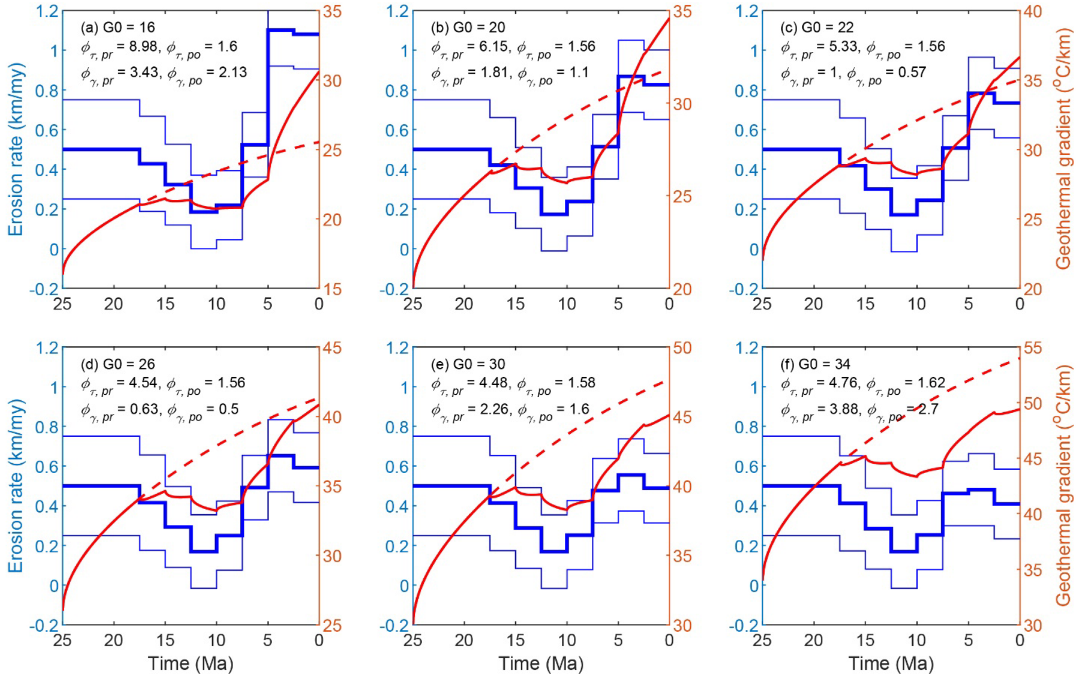
(a) G0 = 16
$\phi_{\tau, pr}$ = 8.98, $\phi_{\tau, po}$ = 1.6
$\phi_{\gamma, pr}$ = 3.43, $\phi_{\gamma, po}$ = 2.13
(b) G0 = 20
$\phi_{\tau, pr}$ = 6.15, $\phi_{\tau, po}$ = 1.56
$\phi_{\gamma, pr}$ = 1.81, $\phi_{\gamma, po}$ = 1.1
(c) G0 = 22
$\phi_{\tau, pr}$ = 5.33, $\phi_{\tau, po}$ = 1.56
$\phi_{\gamma, pr}$ = 1, $\phi_{\gamma, po}$ = 0.57
(d) G0 = 26
$\phi_{\tau, pr}$ = 4.54, $\phi_{\tau, po}$ = 1.56
$\phi_{\gamma, pr}$ = 0.63, $\phi_{\gamma, po}$ = 0.5
(e) G0 = 30
$\phi_{\tau, pr}$ = 4.48, $\phi_{\tau, po}$ = 1.58
$\phi_{\gamma, pr}$ = 2.26, $\phi_{\gamma, po}$ = 1.6
(f) G0 = 34
$\phi_{\tau, pr}$ = 4.76, $\phi_{\tau, po}$ = 1.62
$\phi_{\gamma, pr}$ = 3.88, $\phi_{\gamma, po}$ = 2.7
Erosion rate (km/my)
Geothermal gradient (°C/km)
Time (Ma)

Figure 4

https://doi.org/10.5194/egusphere-2023-2119
Preprint. Discussion started: 9 October 2023

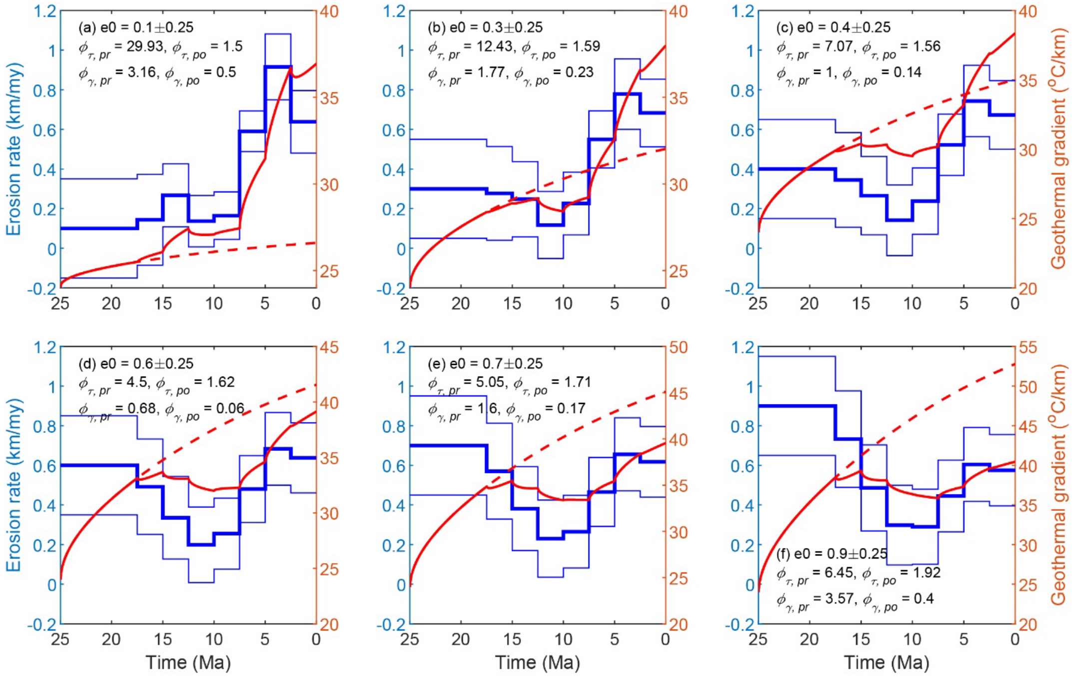

Figure 5

https://doi.org/10.5194/egusphere-2023-2119
Preprint. Discussion started: 9 October 2023

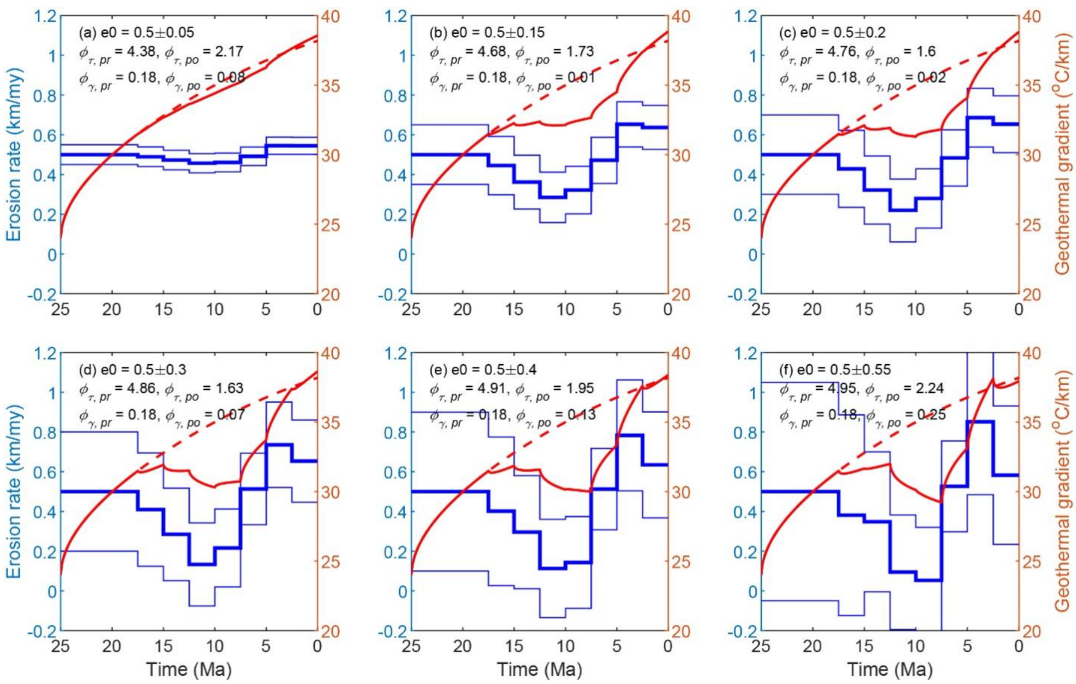

Figure 6

https://doi.org/10.5194/egusphere-2023-2119
Preprint. Discussion started: 9 October 2023

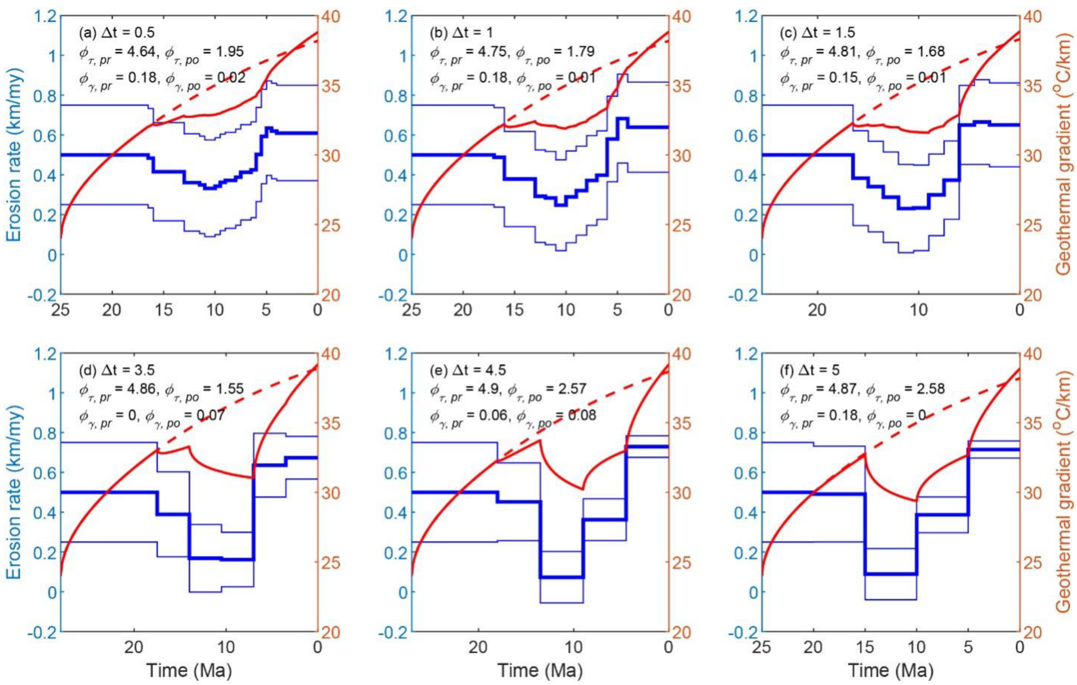

Figure 7

https://doi.org/10.5194/egusphere-2023-2119
Preprint. Discussion started: 9 October 2023

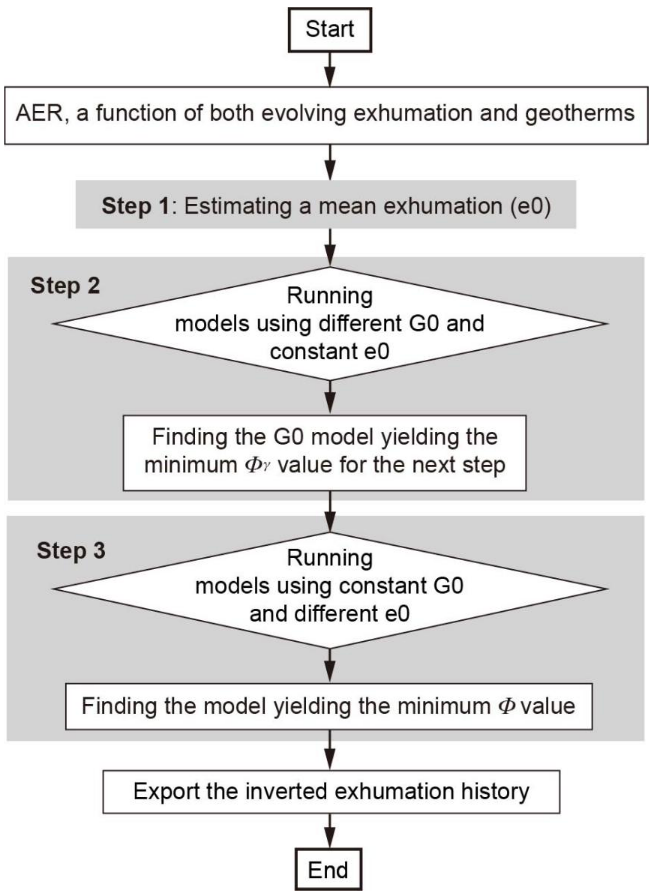

Figure 8

https://doi.org/10.5194/egusphere-2023-2119
Preprint. Discussion started: 9 October 2023

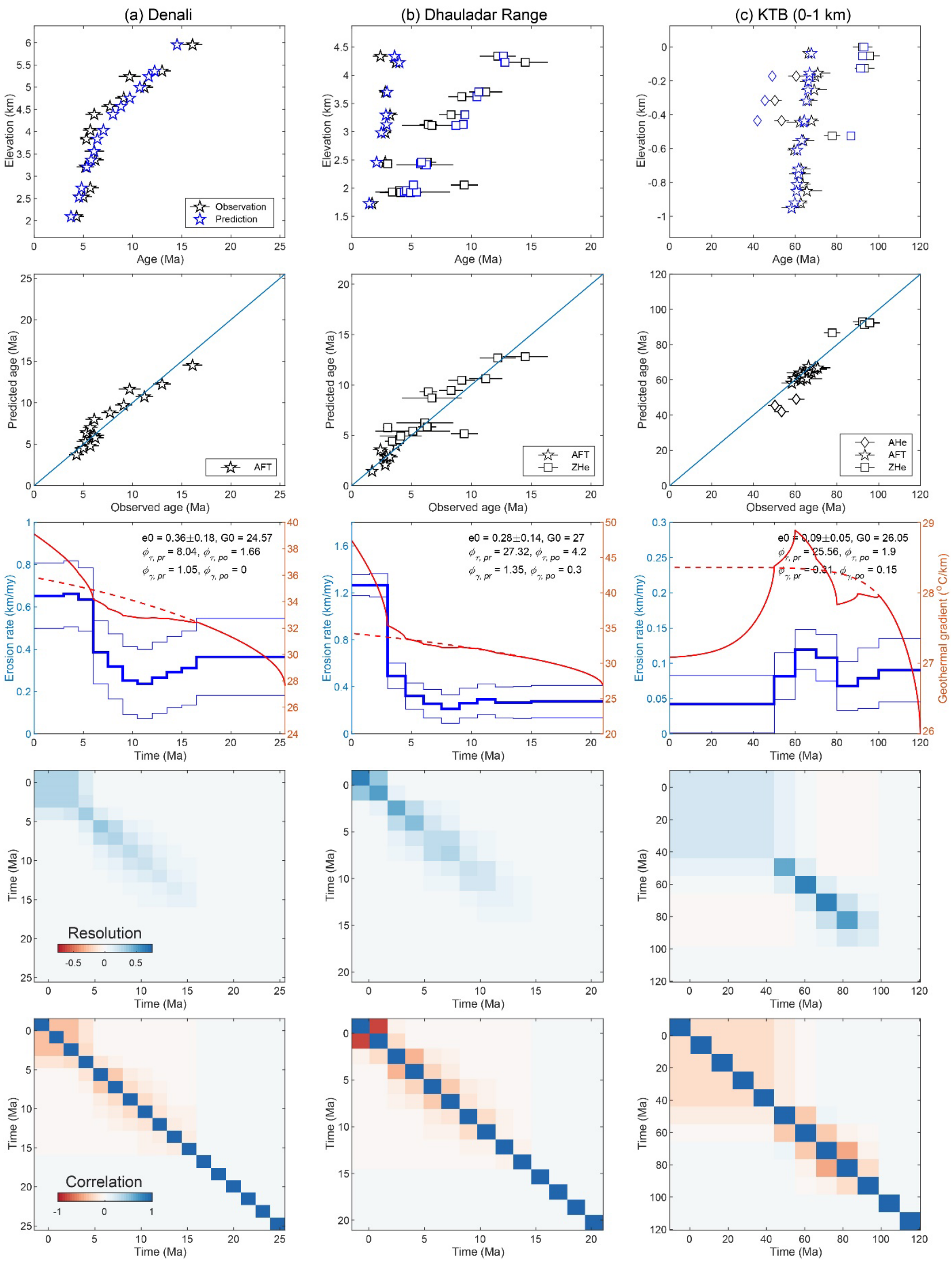

32

33 Figure 9